Scientific Research Publishing

American Journal of Analytical Chemistry, 2026, 17(9), 367-377
https://www.scirp.org/journal/ajac
ISSN Online: 2156-8278
ISSN Print: 2156-8251

Kinetic Validation by MATLAB Simulation of the Ni(III)-HmP Decomposition Step in Nickel-Mediated Histamine Oxidation: Comparison with Thin-Layer Voltammetry

Koita Demo, Mendy Paul*, Diedhiou Moussa Bagha, Sambou Vincent, Diaw Mahy, Sock Oumar

École Supérieure Polytechnique, Université Cheikh Anta DIOP, Dakar, Sénégal
Email: demokoita@gmail.com, *paulsalvador.mendy@gmail.com

How to cite this paper: Demo, K., Paul, M., Bagha, D.M., Vincent, S., Mahy, D. and Oumar, S. (2026) Kinetic Validation by MATLAB Simulation of the Ni(III)-HmP Decomposition Step in Nickel-Mediated Histamine Oxidation: Comparison with Thin-Layer Voltammetry. *American Journal of Analytical Chemistry*, **17**, 367-377.
https://doi.org/10.4236/ajac.2026.179019

Received: August 1, 2026
Accepted: September 15, 2026
Published: September 18, 2026

Abstract

The complexation constant (K) governing the interaction between histamine (Hm) and nickel ions is a critical parameter for developing electrochemical biosensors for food safety monitoring. For the equilibrium $\mathrm{Ni(OH)_2} + \mathrm{Hm} \rightleftharpoons \mathrm{HmNi(II)} + 2\mathrm{OH^-}$, a mass-balance estimate based on our earlier work $K \approx 2.5\times10^{6}$ [1] confirms a strong Hm-Ni(II) affinity; this value is not re-derived here but is used as established context. The specific contribution of the present study concerns the *kinetics* of the subsequent chemical step (decomposition of the Ni(III)-HmP adduct). Thin-layer voltammetry gives $k = (2\pm1)\times10^{-6}$ s^{-1} [1], while an independent MATLAB kinetic simulation (ODE45) of the coupled electrochemical-chemical process reproduces this value with $\mathrm{ksim} = 2.8\times10^{-6}$, in agreement with the experimental rate constant within its reported uncertainty ($k = (2\pm1)\times10^{-6}$ s^{-1}), the agreement being further improved after a 25% thin-layer volume correction. This agreement between an independent numerical model and the experimental kinetics is the central new result of this study, and provides a validated computational framework for future refinement of K from potential-shift data, and for the design of nickel-based electrocatalytic sensors for histamine detection in fish.

Keywords

Histamine, Thin-Layer Voltammetry, Electrocatalytic Sensors, Kinetic Simulation, MATLAB

1. Introduction

Histamine, a biogenic amine formed by the enzymatic decarboxylation of histidine, is a critical indicator of fish freshness and a potent health hazard when concentrations exceed 500 - 1000 mg/kg in seafood [2]-[4]. Elevated histamine levels cause scombroid poisoning, with symptoms ranging from headaches and nausea to severe cardiovascular complications. Regulatory limits vary internationally: the EU, Codex Alimentarius, Australia and New Zealand set a maximum of 200 mg/kg in raw fish, the FDA 50 mg/kg, and the Russian Federation 100 mg/kg for salmon, herring, tuna, and mackerel [5]-[7]. Rapid, accurate, and accessible detection methods are therefore essential for food safety and regulatory compliance.

Traditional analytical techniques (fluorimetry, HPLC, GC) require derivatization, sophisticated instrumentation, and long analysis times (1 - 24 h), limiting their use for routine monitoring [8]-[10]. Electrochemical methods offer a faster, simpler, and field-deployable alternative [11]-[13]. Among these, the electrocatalytic oxidation of histamine mediated by nickel is particularly attractive, since Ni species form complexes with histamine (Hm-Ni(II)) that lower the oxidation overpotential and enhance the electrochemical signal [14]-[16]. This complexation is governed by the equilibrium:

$$\mathrm{Ni(OH)_2} + \mathrm{Hm} \rightleftharpoons \mathrm{Hm\text{-}Ni(II)} + 2\mathrm{OH^-} + 2\mathrm{H^+} \quad (1)$$

where K is the complexation constant, a parameter that governs the sensitivity of the electrocatalytic response. Its strong affinity for Ni^{2+} has been confirmed independently by several groups working with related nickel-histamine systems [17]-[20], but a direct, quantitative link between the electrochemically measured kinetics and a theoretical (simulated) description of the same system has, to our knowledge, not been established.

This study builds directly on our earlier work [1], where the Hm-Ni(II) complex was first identified electrochemically and by NMR, and where the kinetics of its decomposition were characterized by thin-layer voltammetry. The specific, incremental contribution of the present study is to test whether an independent, first-principles MATLAB simulation of the same thin-layer electrochemical-chemical (EC) system can reproduce that previously measured kinetic behavior, and to quantify the agreement between the two approaches. This computational validation is a necessary step distinct from the determination of K itself, which remains a value carried over from our first article and is not re-derived here, before the framework can be used to extract K from potential-shift data in future work.

2. Experimental Part

The experimental setup, reagents, and procedure are identical to those described in detail in our earlier work [1] (Study of the histamine electrochemical oxidation catalyzed by nickel sulfate, Electroanalysis, 2014); only a brief summary and the parameters specific to this study are given here.

Solutions were prepared in double-distilled water using KCl (Acros Organics), trichloroacetic acid (Prolabo), histamine dihydrochloride, $NiSO_4{\cdot}6H_2O$, $HClO_4$, and NaOH (Sigma-Aldrich), all >99% purity.

Measurements used the classical thin-layer three-electrode cell described in our first article [1]: a platinum-grid working electrode sandwiched between two glass microscope slides (thin-layer volume 10 - 50 µL, thickness 100 - 500 µm), a platinum-grid auxiliary electrode, and a saturated calomel reference electrode, controlled by a PGZ 100-Voltalab potentiostat/galvanostat with VoltaMaster 4 software. Full construction details (electrode burning protocol, calliper-based thickness measurement, micropipette filling) are given in our first article [1] and are not repeated here.

Supporting electrolyte was KCl (0.2 M), with NaOH added to fix pH at 12.6; measurements were carried out at 19˚C - 22˚C under aerated conditions, as in our first article [1]. For the present study, voltammograms were recorded at a fixed Ni(II) concentration of 1 $mmol{\cdot}L^{-1}$, while histamine concentration was varied over 1 - 7 $mmol{\cdot}L^{-1}$, a concentration range not covered in our first article [1]. Histamine extraction from sun-exposed fish muscle followed the salting-out/trichloroacetic-acid protocols of Lerke and Bell [21] and Aoua *et al.* [8], as previously applied in our first article [1].

3. Results and Discussion

3.1. Experimental Determination of the Kinetic Behavior of the Hm-Ni(II) System

1) Qualitative evidence of the complexation reaction

Figure 1 below shows the Intensity/Potential curves obtained in a thin layer on platinum with the different reagents.

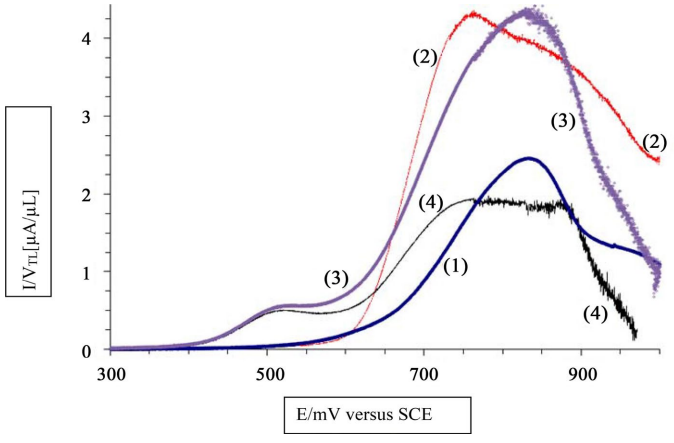

Figure 1. Current potential curves obtained by thin-layer electrochemistry on a platinum anode, with the various reagents involved in this study. KCl = 0.2 M; r = 0.3 mV/s; pH = 12.6. 1): Residual current (Blank). The same curve (as (1)) is obtained in the presence of Hm 10^{-3} M; 2): Solution of curve (1) without Hm + $NiSO_4{\cdot}6H_2O$ 10^{-3} M; 3): Solution of curve (2) + Hm 10^{-3} M; 4): Curve resulting from the subtraction of curve (1) from curve (3).

This figure shows the current-potential curves obtained in thin-layer configuration on platinum with the various reagents (residual electrolyte, Ni(II) alone, and Ni(II) + histamine). As already established in [1], the electrolyte and histamine alone give only the platinum-oxidation signal near 0.55 - 0.9 V; adding Ni(II) produces the Ni(II)/Ni(III) and PtO signals together (0.6 - 1 V); and the ternary mixture (KCl + Ni(II) + histamine) generates an additional, lower-potential signal (0.4 - 0.6 V) that is absent from either reagent alone.

Subtracting the blank from the ternary-mixture curve (curve 4) isolates this signal, which we assign, as in [1], to the oxidation of the Hm-Ni(II) adduct formed via equilibrium (1). This qualitative assignment, together with the complementary NMR evidence, was established and discussed in detail in [1] and is not repeated here.

2) Kinetic rate constant of the Ni(III)-HmP decomposition step

In this section, voltammograms were recorded at increasing histamine concentrations (1, 3, 5, and 7 mmol·L^{-1}) at fixed Ni(II) (1 mmol·L^{-1}). The voltammograms obtained are shown in **Figure 2**.

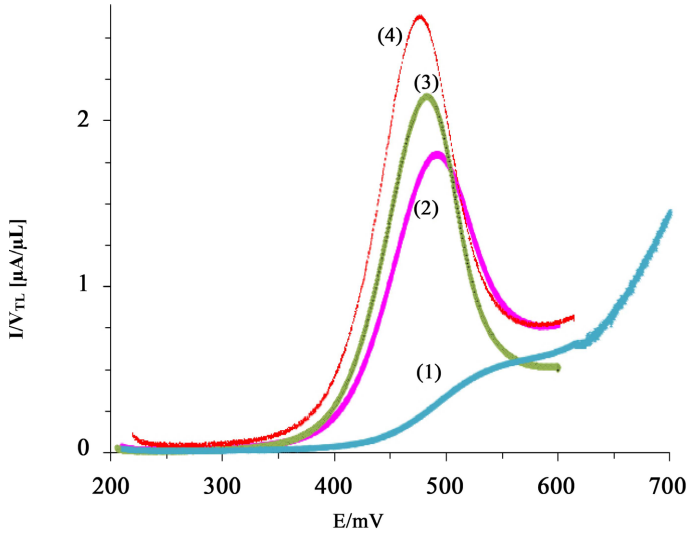

Figure 2. Voltammograms obtained in thin film on a platinum electrode. KCl = 0.2 mol·L^{-1}; r = 0.3 mV/s; pH = 12.6; [$NiSO_4 \cdot 6H_2O$] = 1 mmol·L^{-1}. (1) à (4): [Histamine] respectivement 10^{-3} M, $3 \cdot 10^{-3}$ M, $5 \cdot 10^{-3}$ M et $7 \cdot 10^{-3}$ M.

The Ni(II)-Hm oxidation signal becomes clearly resolved for [Hm] ≥ 3 mmol·L^{-1} and shifts slightly to lower potential with increasing histamine, consistent with the progressive stabilisation of the complex.

The mass balance for the Ni(III)-HmP species in the thin layer, and its resolution using the pseudo-first-order approximation (NaOH in large excess, so [OH^-] is effectively constant), follows exactly the treatment derived and justified in our first work [1] (their Equations (11)-(14)); we do not re-derive it here. Applying that treatment to the present voltammograms gives an apparent rate constant

$k=(2\pm1)\times10^{-6}$ s^{-1}, $k'=4.5\times10^{-8}$ $m^3\cdot mol^{-1}\cdot s^{-1}$ *i.e.*, the same order of magnitude reported for this decomposition step in our first article [1]. We report this value here explicitly as a *consistency check,* as it reproduces, rather than newly discovers, the kinetics of the chemical step and is used as the calibration point against which the independent MATLAB simulation is tested in our first studies.

Applying that treatment point by point to the four voltammograms of **Figure 2** ([Hm] = 1, 3, 5, 7 mmol·L^{-1}) gives a set of independent local estimates of the apparent rate constant, $k=(2\pm1)\times10^{-6}$ s^{-1} (mean ± range), the spread reflecting both the expected [Hm]-independence of this pseudo-first-order constant and the peak-current reproducibility of the technique $\Delta Ipic<5\%$, (three replicate traces per condition) [1]; a further systematic uncertainty of comparable order (~20 - 25%) arises from the thin-layer volume VTL, which enters the underlying mass balance (Equation (10) of our first article) [1], as a direct scaling factor and was itself found to require a 25% correction to reconcile the simulated and experimental current-potential responses.

3) Value of the complexation constant *K*

The complexation constant *K* of equilibrium (1) is a distinct physical quantity from the kinetic rate constant *k* discussed above: *K* describes the *position* of the Hm-Ni(II) complexation equilibrium, whereas *k* describes the *rate* at which the resulting Ni(III)-HmP adduct subsequently decomposes. The two should not be compared directly and are addressed separately here.

An estimate of *K* for this equilibrium was obtained in our earlier work [1] from a mass-balance analysis at a histamine-to-nickel ratio of 10:1 (1 mmol·L^{-1} Hm, 0.1 mmol·L^{-1} Ni(II)), a condition for which the mixture is fully clear (complete dissolution and complexation of Ni(II)). Using the free Ni^{2+} concentration set by the solubility of $Ni(OH)_2$ at pH 12.6 (Ksp ≈ $10^{-14.7}$, giving $[Ni^{2+}]\approx1.3\times10^{-12}$ mol·L^{-1}), this analysis gives: $K\approx2.5\times10^6$, a value corroborated independently, in the same earlier work, by the ≈0.4 V lowering of the oxidation peak potential between free Ni(II) (≈0.9 V) and the Hm-Ni(II) complex (≈0.5 V), which gives $\exp(F\cdot\Delta E/RT)\approx5\times10^6$, the same order of magnitude. Both estimates indicate a strong Hm-Ni(II) affinity. We report this value here as established context from first works [1] rather than as a new result of the present study.

At the working pH of 12.6, Ni(II) is present predominantly as solid/colloidal $Ni(OH)_2$ in the absence of histamine, with a residual free-Ni^{2+} concentration of ≈10^{-12} mol·L^{-1} set by the solubility product [1]; this precipitate dissolves progressively as the histamine-to-nickel ratio increases, becoming fully dissolved and complexed for $[Hm]/[Ni(II)]\geq10$ [1]. Histamine, whose amine pKa values (≈5.8 and ≈9.4) [22]-[24] lie well below the working pH, is essentially fully deprotonated under these conditions. These assumptions justify treating the Hm-Ni(II) complexation equilibrium (1) as essentially complete at high [Hm]/[Ni(II)] ratios and neglecting the free-Ni^{2+} contribution in the kinetic mass balance of Section III.B.

A more rigorous, concentration-resolved determination of *K* specific to the

conditions of Figure 2 (1 mmol·L^{-1} Ni(II), 1-7 mmol·L^{-1} Hm) could be obtained from the dependence of the complex oxidation peak potential Ep on log[Hm], using the *Lingane-type relation*:

$$\mathrm{Ep}\left(\left[\mathrm{Hm}\right]\right)=\mathrm{Ep}\left(0\right)-\left(2.303RT/nF\right)\log K-\left(2.303pRT/nF\right)\log\left[\mathrm{Hm}\right]$$

where the slope of Ep vs. log[Hm] gives the Hm:Ni stoichiometry p, and the intercept gives K.

This refinement is left for future work, pending tabulation of the four Ep values of Figure 2 (currently described only qualitatively in the text); it would be expected, given the same underlying equilibrium, to yield a value consistent with the $\approx 10^6$ order of magnitude established in our first study [1].

3.2. Theoretical (MATLAB) Determination of the Kinetic Behavior

To test independently whether the kinetics established in our first article [1] are compatible with a first-principles description of the coupled electrochemical-chemical (EC) process, the governing differential equation for the Ni(III)-HmP concentration was solved numerically:

$$\frac{\mathrm{d}C}{\mathrm{d}t}=k_1\left(C^0-C\right)\exp\left(k_2\left(k_3+rt\right)\right)-k_4C \quad \text{with } k_1 \text{ - } k_4 \text{ composite constants}$$

derived from the independently known physicochemical parameters of the system (see Table 1 below), integrated with the ODE45 solver in MATLAB. Simulations were run over a range of trial values of the chemical rate constant k until the simulated current matched the experimental voltammetric response (Figure 3).

The composite parameters are $k_1=S\cdot k^0/V_{TL}\left(\mathrm{s}^{-1}\right)$, $k_2=\alpha n_{\lim}F/\left(RT\right)\left(\mathrm{V}^{-1}\right)$, $k_3=E^{0\prime}-E_{I=0}\left(\mathrm{mV}\right)$, and $k_4=k\left(\mathrm{s}^{-1}\right)$, the scanned chemical rate constant, where $E_{I=0}$ is the initial potential of the voltammetric sweep, chosen experimentally low enough that the Faradaic current is essentially zero at $t=0$. For the base-case parameters of Table 1 ($E^{0\prime}$ = 600 mV, $E_{I=0}$ = 225 mV, $n=3$, $\alpha=0.24$, $T=25$˚C), $k_1=1.0352\times10^{-6}$ s^{-1}, $k_2=28.0575$ V^{-1}, $k_3=375$ mV. The model was integrated with the initial condition $C(t=0)=0$, $C^0=5$ mM, scan rate $r=0.3$ mV·s^{-1}, and V_{TL} = 25 µL (base case; corrected by 25% for Figure 5), over the potential window plotted in Figure 3 (200 - 1000 mV, *i.e.* $t\in[0, 2667$ s] at $r=0.3$ mV·s^{-1}), using MATLAB's ODE45 solver (variable-step Runge-Kutta 4(5)) with RelTol = 1 × 10^{-6} and AbsTol = 1 × 10^{-9} (mM), tightened from the ODE45 defaults to resolve the sharp, exponentially amplified peak in $C_0-C(t)$ and confirmed by a tolerance-halving convergence check.

Among the trial values of k explored, ksim was selected as the value for which the simulated C_0-C curve reached the maximum expected conversion ($C_0-C=5$ mM) within the timescale of the potential sweep; the resulting current-potential response was then compared, as an independent check, with the experimental voltammogram (Figure 4 and Figure 5).

Here, $C(t)$ denotes the concentration of Ni(II)-bound histamine not yet converted through the coupled electrochemical-chemical cycle, $C_0=5$ mM is the total

initial concentration engaged in the cycle (Table 1), and $C_0 - C$ is the cumulative concentration of histamine consumed; complete conversion therefore corresponds to $C \to 0$.

Table 1. Experimental data.

C^0 (mM)	$E^{0\prime}$ (mV)	$E_{I=0}$ (mV)	N	α	k_1 (s^{-1})	k_2 (V^{-1})	k_3 (mV)	k (mol/m^3/s)	V_{TL} (µL)
5	600	225	3	0.24	10352.10^{-6}	28,0575	375	?	25 µL

The principal objective is to determine the value of the rate constant k for which complete depletion of histamine is achieved, *i.e.*, when the concentration of histamine reaches $C = 0$, corresponding to $C_0 - C = 5$ mM.

The variable C used above to denote the Ni(III)-HmP adduct concentration in this single-step mass balance is distinct from the cumulative histamine-conversion variable C introduced in Section III.B.

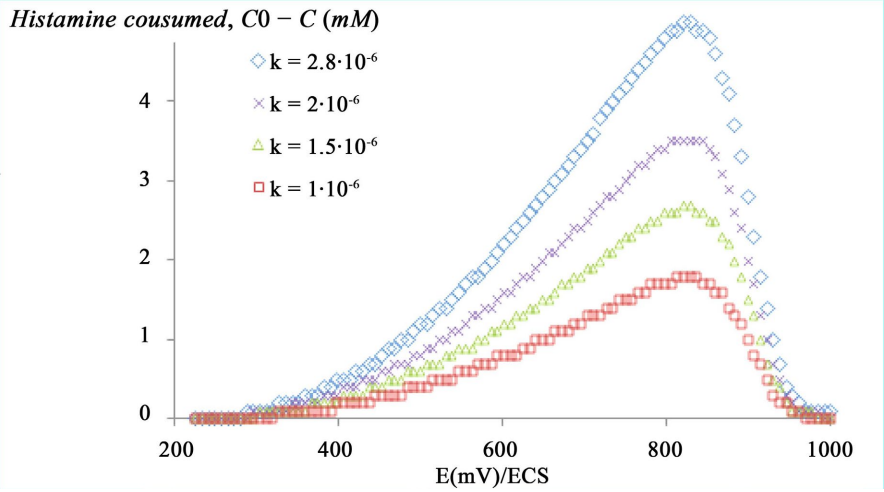

Figure 3. Theoretical concentration curves of $C_0 - C$ for histamine obtained from MATLAB simulations.

The best agreement, corresponding to complete histamine consumption over the timescale of the experiment, was obtained for: ksim = 2.8 × 10^{-6}.

This value is of the same order of magnitude as, and within experimental uncertainty of, the $k = (2 \pm 1) \times 10^{-6}$ s^{-1}, obtained independently by thin-layer voltammetry in [1]. This numerical reproduction of an experimentally established rate constant, from a first-principles kinetic model built independently of the voltammetric fitting procedure of our first work [1], is the principal new result of this study.

3.3. Comparison between Experimental and Simulated Current-Potential Responses

Using $\text{ksim} = 2.8 \times 10^{-6}$, the current I was recalculated from the electrochemical

rate expression.

$I = nFSk^0C' \exp\left(\frac{\alpha n_{\lim} F}{RT}\right) \times \left(E_{I=0} - E^{0\prime} + rt\right)$ and compared to the experimental voltammogram (Figure 4 below).

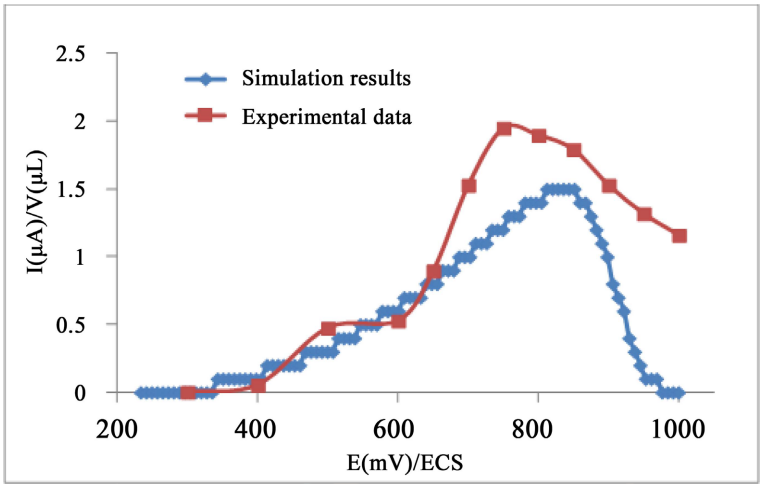

Figure 4. Comparison of the experimental results with the theoretical results obtained from the simulation for $k = 2.8 \times 10^{-6}$.

The two curves agree well overall, but with $a \approx 100$ mV shift in peak potential and a slightly higher experimental peak current, attributable to the sensitivity of thin-layer measurements to small volumetric uncertainties, and to a likely overestimation of the effective thin-layer volume in the model. Correcting this volume by 25% substantially improves the agreement (Figure 5 below), supporting the validity of the simulation for describing histamine oxidation kinetics under these conditions.

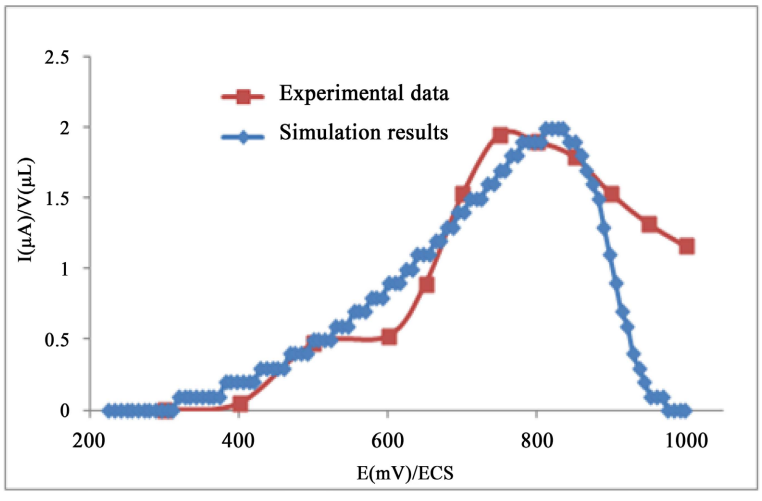

Figure 5. Comparison of the experimental results with the theoretical results obtained from the simulation for $k = 2.8 \times 10^{-6}$, with correction of the thin-layer volume.

4. Conclusions

This study reproduces, by an independent MATLAB kinetic simulation, the rate constant governing the decomposition of the Ni(III)-HmP adduct that we first measured electrochemically in our first article [1] ($k = (2 \pm 1) \times 10^{-6}$ s^{-1} experimentally, ksim $= 2.8 \times 10^{-6}$ from simulation), with good agreement after a 25% thin-layer volume correction. This computational validation provides a tested numerical framework for the coupled electrochemical-chemical kinetics of histamine oxidation by nickel.

The complexation constant K of equilibrium, a separate thermodynamic quantity from the kinetic rate constant k, was estimated in our earlier work [1] at $K \approx 2.5 \times 10^{6}$ (mass-balance analysis, corroborated by an independent peak-potential estimate), confirming a strong Hm-Ni(II) affinity; refining this value specifically for the conditions of **Figure 2**, via the peak-potential/log [Hm] (Lingane) treatment is identified as a direct next step. Together, these results strengthen the case for nickel-based electrochemical biosensors for histamine detection in food safety applications.

Acknowledgements

This research was funded by the Senegalese government through the LEPM laboratory of Cheikh Anta Diop University.

Author Contributions

Conceptualization, Koita Demo, Mendy Paul, and Diaw Mahy; methodology, Koita Demo, Mendy Paul, Diaw Mahy, and Sock Oumar; software, Koita Demo, Mendy Paul, and Diedhiou Moussa Bagha; validation, Diaw Mahy, Sock Oumar, and Sambou Vincent; formal analysis, Koita Demo, Mendy Paul, and Diedhiou Moussa Bagha; investigation, Koita Demo, Mendy Paul, and Diedhiou Moussa Bagha; resources, Koita Demo, Mendy Paul, and Diedhiou Moussa Bagha; data curation, Koita Demo, Mendy Paul, and Diedhiou Moussa Bagha; writing—original draft preparation, Koita Demo, Mendy Paul, and Diedhiou Moussa Bagha; writing—review and editing, Koita Demo, Mendy Paul, and Diedhiou Moussa Bagha; visualization, Diaw Mahy, and Sock Oumar; supervision, Diaw Mahy, and Sock Oumar; project administration, Sambou Vincent, and Diaw Mahy; funding acquisition, Sambou Vincent. All authors have read and agreed to the published version of the manuscript.

Conflicts of Interest

The authors declare no conflicts of interest regarding the publication of this paper.

References

[1] Koita, D., Tzedakis, T., Kane, C., Diaw, M., Sock, O. and Lavedan, P. (2014) Study of the Histamine Electrochemical Oxidation Catalyzed by Nickel Sulfate. *Electroanalysis*, **26**, 2224-2236. https://doi.org/10.1002/elan.201400155

[2] FAO (2013) Highlights. Public Health Risks of Histamine and Other Biogenic Amines from Fish and Fishery Products. https://openknowledge.fao.org/items/4b5ad160-b0d3-4a4c-9cb5-2c036bf71a34

[3] FDA (2024) CPG Sec 540.525 Scombrotoxin (Histamine)-Forming Fish and Fishery Products—Decomposition and Histamine (CPG 7108.24). https://www.fda.gov/regulatory-information/search-fda-guidance-documents/cpg-sec-540525-scombrotoxin-histamine-forming-fish-and-fishery-products-decomposition-and-histamine

[4] Zhernov, Y.V., Simanduyev, M.Y., Zaostrovtseva, O.K., Semeniako, E.E., Kolykhalova, K.I., Fadeeva, I.A., *et al.* (2023) Molecular Mechanisms of Scombroid Food Poisoning. *International Journal of Molecular Sciences*, **24**, Article 809. https://doi.org/10.3390/ijms24010809

[5] Visciano, P., Schirone, M. and Paparella, A. (2020) An Overview of Histamine and Other Biogenic Amines in Fish and Fish Products. *Foods*, **9**, Article 1795. https://doi.org/10.3390/foods9121795

[6] de la Torre, C.A.L. and Conte-Junior, C.A. (2018) Detection of Biogenic Amines: Quality and Toxicity Indicators in Food of Animal Origin. In: *Food Control and Biosecurity*, Elsevier, 225-257. https://doi.org/10.1016/b978-0-12-811445-2.00006-4

[7] Verkhivker, Y. and Altman, E. (2018) Influence Parameters of Storage on Process of Formation the Histamine in Fish and Fish Products. *Journal of Water Resources and Ocean Science*, **7**, 10-14. https://doi.org/10.11648/j.wros.20180701.12

[8] Aoua, C., Yacoubi, B. and Zekhnini, A. (2024) Development of a New Method for Extracting Histamine from Marine Fish Flesh Using the Salting-Out Technique. *Italian Journal of Food Safety*, **13**, Article 12117. https://doi.org/10.4081/ijfs.2024.12117

[9] Ahangari, H., Tavassoli, M., Khezerlou, A., Kiani Salmi, N., Ehsani, A. and Afshar Mogaddam, M.R. (2023) A Review on the Determination of Biogenic Amines in Fresh and Processed Fish Products Using HPLC, LC-MS/MS and Other Chromatographic Methods. *Combinatorial Chemistry & High Throughput Screening*, **26**, 2598-2606. https://doi.org/10.2174/1386207326666230316141040

[10] Mairal-Lerga, T., Bermudo Redondo, M.C., Skouridou, V., Jauset-Rubio, M. and O'Sullivan, C.K. (2025) Aptamer Lateral Flow Assay for the Rapid Detection of Histamine in Fish and Human Blood. *Journal of Hazardous Materials*, **494**, Article 138540. https://doi.org/10.1016/j.jhazmat.2025.138540

[11] Munir, M.A., Rahmawati, F., Jamal, J.A., Ibrahim, S., Said, M.M. and Ahmad, M.S. (2023) Inspecting Histamine Isolated from Fish through a Highly Selective Molecularly Imprinted Electrochemical Sensor Approach. *ACS Omega*, **8**, 13352-13361. https://doi.org/10.1021/acsomega.3c00768

[12] Aoki, H., Miyazaki, R. and Einaga, Y. (2025) Non-Enzymatic Selective Detection of Histamine in Fishery Product Samples on Boron-Doped Diamond Electrodes. *Biosensors*, **15**, Article 489. https://doi.org/10.3390/bios15080489

[13] Singh, D., Srivastava, A., Chaturvedi, V.K. and Singh, J. (2025) Nanostructured WS_2@Chitosan-Modified Screen-Printed Carbon Electrodes for Efficient Amperometric Detection of Histamine. *ACS Omega*, **10**, 3153-3164. https://doi.org/10.1021/acsomega.4c10419

[14] Xu, Y., Cheng, Y., Jia, Y. and Ye, B.C. (2020) Synthesis of MOF-Derived Ni@C Materials for the Electrochemical Detection of Histamine. *Talanta*, **219**, Article 121360. https://doi.org/10.1016/j.talanta.2020.121360

[15] Yang, J., Hu, C., Huang, H., Yang, H., Li, L., Yao, W., *et al.* (2025) Efficient and Highly Sensitive Electrochemical Histamine Detection in Fish on NiO/Cu/Cu_2O Heterojunc-

tion Electrode with Tunable Oxygen Vacancy Density by Electrodeposition Technique. *Microchemical Journal*, **218**, Article 115545. https://doi.org/10.1016/j.microc.2025.115545

[16] Mansilungan, M.D. (2025) Electrochemical Histamine Sensor Based on Nickel Hexacyanoferrate-Modified Glassy Carbon Electrode. Master's Theses, De La Salle University.

[17] Švarc-Gajić, J. and Stojanović, Z. (2010) Electrocatalytic Determination of Histamine on a Nickel-Film Glassy Carbon Electrode. *Electroanalysis*, **22**, 2931-2939. https://doi.org/10.1002/elan.201000352

[18] Fukushima, Y. and Aikawa, S. (2021) Colorimetric Sensing of Histamine in Aqueous Solution by a System Composed of Alizarin Complexone and Ni^{2+} Complex via Indicator Displacement Approach. *Tetrahedron Letters*, **72**, Article 153088. https://doi.org/10.1016/j.tetlet.2021.153088

[19] Li, P., Zhou, B., Ge, M., Jing, X. and Yang, L. (2022) Metal Coordination Induced SERS Nanoprobe for Sensitive and Selective Detection of Histamine in Serum. *Talanta*, **237**, Article 122913. https://doi.org/10.1016/j.talanta.2021.122913

[20] Hadi, M. and Mostaanzadeh, H. (2018) Sensitive Detection of Histamine at Metal-Organic Framework (Ni-BTC) Crystals and Multi-Walled Carbon Nanotubes Modified Glassy Carbon Electrode. *Russian Journal of Electrochemistry*, **54**, 1045-1052. https://doi.org/10.1134/s1023193518120066

[21] Lerke, P.A. and Bell, L.D. (1976) A Rapid Fluorometric Method for the Determination of Histamine in Canned Tuna. *Journal of Food Science*, **41**, 1282-1284. https://doi.org/10.1111/j.1365-2621.1976.tb01152.x

[22] Heidarzadeh-Asl, S., Maurer, M., Kiani, A., Atiakshin, D., Stahl Skov, P. and Elieh-Ali-Komi, D. (2025) Novel Insights on the Biology and Immunologic Effects of Histamine: A Road Map for Allergists and Mast Cell Biologists. *Journal of Allergy and Clinical Immunology*, **155**, 1095-1114. https://doi.org/10.1016/j.jaci.2024.12.1081

[23] Jezuita, A., Makowska-Janusik, M., Ejsmont, K. and Marczak, W. (2025) Substituent Effect in Histamine and Its Impact on Interactions with the G Protein-Coupled Human Receptor H1 Modelled by Quantum-Chemical Methods. *Molecules*, **30**, Article 3736. https://doi.org/10.3390/molecules30183736

[24] Li, H., Regaldo, D., Wu, C.J., Prato, M., Treglia, A., Wang, H., *et al.* (2025) Design of Strong and Weak Intermolecular Interactions to Engineer Buried Interfaces in Inverted Wide-Bandgap Perovskite Solar Cells. *Energy & Environmental Science*, **18**, 6618-6627. https://doi.org/10.1039/d5ee01110h